JCTC Journal of Chemical Theory and Computation

ARTICLE

pubs.acs.org/JCTC

Spectroscopic Properties of Azobenzene-Based pH Indicator Dyes: A Quantum Chemical and Experimental Study

Daniel Escudero,[†] Sabine Trupp,[‡] Beate Bussemer,[§] Gerhard J. Mohr,[‡] and Leticia González*[,†]

[†]Institute of Physical Chemistry, Theoretical Chemistry, Friedrich-Schiller University Jena, Helmholtzweg 4, D-07743 Jena, Germany

[‡]Department of Polytronic Systems, Workgroup Sensor Materials, Fraunhofer Research Institution for Modular Solid State Technologies (EMFT), Josef-Engert Strasse 9, D-93053 Regensburg, Germany

[§]Institute of Physical Chemistry, Friedrich-Schiller University Jena, Lessingstrasse 10, D-07743 Jena, Germany

ABSTRACT: The UV−visible absorption spectra of six new optical sensors based on acidochromic azobenzenes have been measured and assigned with the help of quantum chemical calculations. The investigated compounds are able to monitor the pH in the range from pH 3−10. Using the hybrid density functional PBE0 and including solvent effects with a polarized continuum model, the agreement between the experimental and theoretical UV/vis spectra of the dyes in their neutral and anionic forms is very good. The spectroscopic $\pi\pi^*$ states, responsible for the optical properties of the sensors, are described within an accuracy of 0.1 eV. Similar accuracy is demonstrated in the $n\pi^*$ states. The $\pi\pi^*$ states can be assigned as a charge transfer from the aromatic π orbital localized in the azo-phenol moiety to the antibonding π^* of the azo group. Under basic conditions, the spectrum is bathochromically shifted and more intense than in acid media. Upon substitution in the phenyl moiety, red- or blue-shifts of the UV−visible bands are observed depending on whether the substituent is electron-donor or -withdrawing, respectively. These effects are stronger at high pH values and can be rationalized in terms of the stabilization and/or destabilization of the involved frontier orbitals.

1. INTRODUCTION

The development of pH sensors is a continuous challenge in chemistry.[1] Although the determination of pH with traditional electrochemical sensors is well-established, optical sensors are a valuable alternative where glass electrodes are impractical or impossible to use.[2] Moreover, optical sensors can be more versatile than electrodes, as they are easy and inexpensive to fabricate,[3] and profit from the current advances of optical spectroscopy.

Azobenzene and derivatives have attracted a considerable amount of attention due to their capability to reversibly switch between the cis and trans conformers using two different wavelengths,[4] and therefore their large applicability as molecular devices.[5] They are used as light-driven membranes,[6] as single-molecule optomechanical machines,[7] as media storage,[8] or to control peptide folding.[9] Moreover, because they allow for facile and multiple functionalizations, a wide range of azobenzene-based indicator dyes have been synthesized, initially for detecting alkali, earth alkali, and heavy metal ions,[10] but later also for monitoring electrically neutral and anionic analytes such as alcohols,[11] amines,[12] aldehydes,[13] saccharides,[14] and bisulfite.[15] Recently, some of us have synthesized new derivatives of 2-hydroxyethylsulfonyl azobenzene (HESAB) indicator dyes with emphasis on measuring the pH in range between 3 and 10.[16] These indicators can be covalently linked to polymers containing hydroxyl functions such as cellulose, polyurethane hydrogel, and hydroxyalkyl methacrylate. Because one of our aims is to design indicator dyes, which exhibit strong color changes in this pH range, the goal of this Article is to present a comprehensive study of the substitution effects on the spectral properties of the corresponding protonated and deprotonated forms of HESAB. In particular, we want to predict whether or not the absorbance spectra of the phenolic dyes in going from acid to base form (i.e., protonated to deprotonated form) are well separated, thus providing indicator materials whose color changes can be easily distinguished and quantified by optical sensor modules.

To shed some light into the photophysics of the HESAB compounds, which can in turn help to predict the potential use of these dyes as pH indicators, the experimental spectra have been characterized with the help of quantum chemical calculations. While recording absorption spectra can be close to routine, the computation of electronically excited states of large organic dyes with chemical accuracy (less than 0.1 eV) is still a challenging problem in modern quantum chemistry. Currently, time-dependent density functional theory (TD-DFT) is the most extended theoretical tool to compute transition energies and oscillator strengths in organic and inorganic compounds.[17] Although the performance of different functionals may vary depending on the treated systems,[18] it seems that corrected hybrid functionals are best suited to describe the excited states of delocalized aromatic dye systems,[19] and this approach is used here.

2. EXPERIMENTAL SECTION

Sample Preparation. The six azobenzene dyes (**1**−**6**) with their deprotonated forms (**1**$^-$ −**6**$^-$) shown in Figure 1 were investigated. The azo function is in para position to the phenol hydroxyl group. Substitution effects are studied by substituting H by two electron donors (CH_3, OCH_3) and/or two electron-withdrawing (F, Br) substituents on the phenyl moiety.

Received: December 16, 2010
Published: March 09, 2011

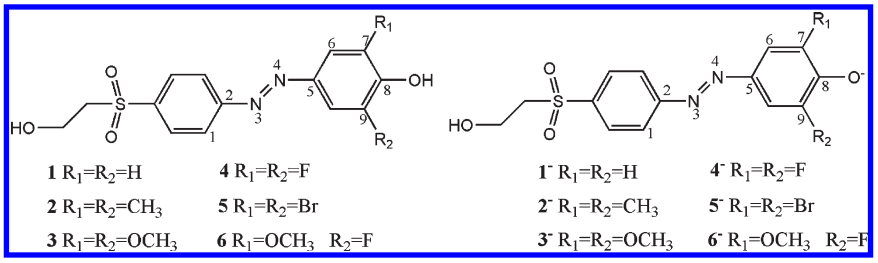

Figure 1. Chemical structure of the 2-hydroxyethylsulfonyl azobenzene dyes here investigated.

Table 1. Main Geometrical Parameters of Gas-Phase-Optimized Compounds 1−6 and 1^-−6^-[a]

compound	d_{3-4}[b]	d_{2-3}[b]	d_{4-5}[b]	d_{6-7}[b]	d_{8-9}[b]	α_{2-3-4}[c]	α_{3-4-5}[c]	$\tau_{1-3-4-6}$[c]
azobenzene								
RI-BP86/TZVP[d]	1.267	1.417	1.417			114.8	114.8	180
PBE0/TZVP	1.243	1.413	1.413	1.386	1.393	115.1	115.1	180
X-ray[e]	1.247	1.428	1.428	1.384	1.391	114.1	114.1	178.1
1 (PCM-PBE0/TZVP)	1.248	1.413	1.399	1.380	1.401	114.7	116.2	170.5
1 (PBE0/TZVP)	1.271	1.418	1.408	1.390	1.410	114.2	115.4	167.5
2	1.246	1.412	1.402	1.384	1.405	114.5	115.7	163.2
3	1.247	1.410	1.400	1.388	1.404	114.3	115.8	162.3
4	1.244	1.412	1.405	1.377	1.397	114.6	115.2	165.7
5	1.244	1.412	1.405	1.377	1.397	114.6	115.2	165.7
6	1.245	1.412	1.403	1.386	1.392	114.4	115.6	166.2
$\mathbf{1}^-$ (PCM-PBE0/TZVP)	1.276	1.395	1.361	1.368	1.448	114.0	117.2	178.8
$\mathbf{1}^-$ (PBE0/TZVP)	1.288	1.377	1.344	1.359	1.459	113.7	117.4	173.1
$\mathbf{2}^-$ (PCM-PBE0/TZVP)	1.282	1.390	1.357	1.369	1.457	114.0	117.2	178.6
$\mathbf{2}^-$(PBE0/TZVP)	1.289	1.376	1.344	1.361	1.465	113.7	117.5	172.9
$\mathbf{3}^-$	1.295	1.370	1.339	1.361	1.471	113.8	117.1	172.6
$\mathbf{4}^-$	1.283	1.380	1.347	1.355	1.459	113.8	117.1	171.4
$\mathbf{5}^-$	1.277	1.386	1.354	1.359	1.466	113.9	117.2	170.9
$\mathbf{6}^-$	1.289	1.375	1.343	1.363	1.456	113.9	117.2	171.8

[a] Theoretical and experimental values of *trans*-azobenzene are given for comparison. The corresponding chemical structures with the atom numbering can be found in Figure 1. [b] Distances in angstroms. [c] Angles in degrees. [d] Values obtained under C_{2h} symmetry constraint from ref 29. [e] Experimental values from ref 28.

The synthesis of the 2-hydroxyethylsulfonyl azo dye **1** was accomplished by diazotation of 2-(4-aminobenzenesulfonyl)-ethanol to phenol in acetic acid. The product was precipitated as fine yellow-orange powder. Yield: 28%. Anal. Calcd for $C_{14}H_{14}N_2O_4S$ (306.34 g/mol): C; 54.89%; H, 4.61%; N, 9.14%; S, 10.47%. Found: C, 54.89%; H, 4.53%; N, 9.10%; S, 10.72%. ^{1}H NMR (DMSO): δ (ppm) 7.85−8.07 (m, 6H, =CH−), 6.98 (m, 2H, =CH−), 3.74 (t, 2H, $-CH_2-$), 3.51 (t, 2H, $-CH_2-$). Mass spectrometry data (EI): *m*/*e* (%), 306 (38). The synthesis of the 2-hydroxyethylsulfonyl azo dyes **2**−**6** has been described in detail elsewhere.[13]

Spectroscopic Measurements. The absorbance spectra of the dissolved dyes **1**−**6** were recorded on a Lambda 16 UV−vis spectrometer (Perkin-Elmer) at 20 ± 2 °C. The dyes were dissolved in methanol and mixed with the aqueous buffered solutions in a 1:1 ratio because of the low solubility of the dyes in pure aqueous solution. A wide pH range buffer was used, which was 0.04 M in sodium acetate, 0.04 M in boric acid, 0.04 M in sodium dihydrogen phosphate, and 0.1 M in sodium sulfate. The pH was adjusted in a way that exclusively the neutral or the anionic form of the dyes was observed.

3. COMPUTATIONAL DETAILS

For the sake of computational ease, the 2-hydroxyethyl function was replaced by a methyl group in all of the calculations (see Figure 1). The resulting geometries were optimized in the trans configuration using the global hybrid functional PBE0[20] in combination with a polarized valence triple-ζ basis set (TZVP) for all atoms. The nature of the stationary points was confirmed by calculating the Hessian at the same level of theory. The calculation of the transition energies and oscillator strengths was done with the same functional. With 25% of exact Hartree−Fock exchange, PBE0 was chosen because it delivers excitation energies with mean absolute errors of 0.14 eV for organic dyes.[19b] The effect of the methanol environment on the excitations energies was modeled with the polarized continuum model (PCM)[21] and ε = 32.6. For reference, the UV spectrum of the unsubstituted compounds **1**/$\mathbf{1}^-$ is also calculated using correlated ab initio second-order approximated coupled-cluster theory[22] in the resolution of the identity approximation (RI-CC2)[23] and the pure functional BP86[24,25] also within RI approximation. The effect of the solvent on the geometries was also investigated at the PBE0 level of theory. RI-BP86 and

dx.doi.org/10.1021/ct1007235 |*J. Chem. Theory Comput.* 2011, 7, 1062–1072

Table 2. UV/Vis Experimental Data of HESAB Compounds 1−6 under Acid and Basic Conditions (pH Is Also Given) Measured in Buffered Methanol (v/v = 1:1)[a]

	1 λ_{max}	2 λ_{max}	3 λ_{max}	4 λ_{max}	5 λ_{max}	6 λ_{max}
acid	pH = 3.52	pH = 3.17	pH = 4.16	pH = 3.19	pH = 3.19	pH = 3.16
	456, 361 (2.72, 3.44)	373 sh, 427 (3.32 sh, 2.91)	460 sh, 395 (2.70 sh, 3.14)	355 (3.49)	354 (3.50)	374 (3.32)
basic	pH = 11.08	pH = 11.28	pH = 10.83	pH = 11.44	pH = 11.54	pH = 11.28
	460 (2.70)	499 (2.49)	525 (2.36)	444 (2.79)	460, 292 (2.70, 4.25)	487(2.55)

[a] Maximum absorption peaks and most relevant shoulders (sh) in nm and in eV in parentheses.

Table 3. Molar Extinction Coefficients of the Dyes in Pure Methanol[a]

	ε [L mol^{-1} cm^{-1}]			
	neutral form	anionic orm	λ_{max} neutral form [nm]	λ_{max} anionic form [nm]
1/**1**$^-$	27 300	27 700	364	441
2/**2**$^-$	24 190	29 240	373	498
3/**3**$^-$	18 890	36 090	396	522
4/**4**$^-$	25 200	30 000	354	440
5/**5**$^-$	14 430	21 740	354	452
6/**6**$^-$	19 740	30 730	375	485

[a] The neutral form was obtained by addition of 100 μL of 0.1 M hydrochloric acid, while the anionic form was obtained by addition of 100 μL of triethylamine.

RI-CC2 calculations were performed with the TURBOMOLE.5.10 program package,[26] while the rest of calculations were performed with Gaussian 03.[27]

4. RESULTS AND DISCUSSION

Structure of Azo-vinyl Sulfonyl Dyes. The most relevant geometrical parameters of the studied compounds **1**−**6** and corresponding anions are collected in Table 1. For the sake of comparison, azobenzene in the *trans*-conformation is also included. The low-lying excited states of azobenzene (and derivatives) involve the antibonding orbital located in the N═N bond; therefore, it is important to describe this bond length properly. Experimentally, the N═N distance of azobenzene is 1.247 Å.[28] Hättig et al. showed that triple-ζ basis sets are indispensable for an accurate description of this bond.[29] It has been estimated that RI-BP86/TZVP level of theory delivers bond distances in azobenzene ca. 0.001 Å larger than MP2 but very similar to the crystal structure.[29] As we see in Table 1, RI-BP86/TZVP overestimates the N═N bond (d_{3-4}) by ca. 0.02 Å. Interestingly, the result of the hybrid functional PBE0 (1.243 Å) is in much better agreement with the X-ray distance. The adjacent N−C bonds (d_{2-3} and d_{4-5}) are underestimated by both BP86 and PBE0 by ca. 0.01 Å. Despite being noticeable, these discrepancies are within the error bar of the experiment.[28]

In view of the previous results and because no X-ray structures are available for HESAB derivatives to compare, we shall consider 0.01 Å as the error bar for the geometries of the HESAB compounds obtained with PBE0/TZVP. The N═N bond in the unsubstituted HESAB compound **1** is larger than in azobenzene and further destabilized upon deprotonation. Interestingly, when the solvent is included in the optimization (PCM-PBE0 values), the azo bond (d_{3-4}) is compressed in the neutral and anionic forms, while the bonds nearby (d_{2-3} and d_{4-5}) are almost unaffected in the neutral form but stretched by ca. 0.02 Å in the anion.

The changes in the bond angles are negligible in both neutral and ionic forms (see α values in Table 1). In contrast, the planarity of these compounds deserves some attention. Despite some controversy,[30] nowadays it seems well-accepted that azobenzene is planar in the gas phase, as suggested by early X-ray experiments[28] and confirmed by accurate MP2 calculations.[29,31] Simple substituted 4,4′-azobenzene derivatives are also planar at both MP2 and DFT levels of theory if the basis set is sufficiently large. On the contrary, if a smaller basis set, that is, MP2/6-31+G(d) level of theory is used, significantly twisted geometries, with a dihedral angle of ca. 20°, are predicted.[30] The dyes investigated here are twisted by ca. 15° (see dihedral $\tau_{1-3-4-6}$ in Table 1). Because we employ the flexible TZ basis set, we are confident that the nonplanarity of HESAB systems in vacuum is physical and due to the bulky nature of the substituents. We note that the frequencies corresponding to the out-of-plane motion of the rings are very small (e.g., 62 and 105 cm^{-1} in compound **1** and of similar magnitude or even smaller in the other neutral species), increasing the possibility that nonplanar geometries contribute to the experimental absorption spectrum (see below). Worth mentioning is that a certain degree of planarity is recovered upon deprotonation and that the **1**/**1**$^-$ and **2**$^-$ optimized structures in the presence of solvent are slightly more planar than in the gas phase (see Table 1). These effects are especially important to address properly the nπ^* excitations of HESAB compounds, as we shall discuss below.

The rest of the compounds have been optimized only at the PBE0/TZVP level of theory. In the neutral HESAB, the calculated values for N═N and adjacent C−N bonds (now asymmetric), as well as the angle between them, are very similar to those of azobenzene (see Table 1). Both the electron donor (**2** and **3**) and the electron acceptor (**4** and **5**) substituents have little effect on the geometry of the neutral (or the anionic) HESAB. However, there are interesting changes upon deprotonation. In the phenolate form, a strong resonance effect through the conjugated system can be observed, which strongly influences the geometry in two ways: On the one hand, the N═N bond is activated, see that the distance of the azo moiety is enlarged in comparison to the neutral forms by 0.03−0.05 Å, and, on the other hand, the aromaticity of the ring decreases, see the different alternate C−C distances of the phenyl group. Also significant is that the planarity of the HESAB increases in the anionic forms. For instance, in the neutral form **3** the dihedral angle $\tau_{1-3-4-6}$ is 17.4°, while in **3**$^-$ it decreases to 6.8°.

UV−Visible Absorption Spectroscopy. Experimentally, the UV/vis spectra of these compounds (with 2-hydroxyethyl moieties, vide supra) are recorded in methanol/buffer (1:1) of different pH values. The experimental maximum absorption peaks of compounds **1**−**6** at specific pH values measured in buffered aqueous methanol are collected in Table 2, and the molar extinction coefficients in pure methanol solutions are given in Table 3.

Before discussing the assignment of the different spectra based on quantum chemical calculations, it is worth reviewing the spectrum of azobenzene, which has been the subject of extensive studies.[29−32] In the gas phase, the absorption spectrum is characterized by a weak nπ^* transition at 2.82 eV (440 nm) followed by a strong $\pi\pi^*$ state peaking at 4.12 eV (301 nm).[33] CC2 calculations deliver values of 2.84 and 4.04 eV, respectively, in very good agreement with the experimental values.[29] The employment of TD-DFT in azobenzene and derivatives is, however, not straightforward. Charge transfer (CT) states are typically very much underestimated due to the wrong long-range behavior of the applied standard exchange-correlation functionals.[34] Several strategies have emerged to consider long-range effects. For instance, range-separated functionals where the total exchange energy is split into short- and long-range contributions have been developed; examples of these functionals are LC-wB97,[35] LC-wB97XD,[36] or CAM-B3LYP.[37] Another possibility is to use hybrid functionals where the exact Hartree−Fock exchange is modified; an illustration is the PBE0 functional, which contains 25% of exact HF exchange. As expected, pure functionals deliver rather poor values in azobenzene. RI-BP86/aug-TZVP predicts the two transitions of azobenzene at 2.19 and 3.35 eV; that is, both bands are underestimated by more than 0.5 eV.[29] The hybrid functional B3LYP red-shifts experimental values to a lesser extent, but it still accounts for errors of 0.3−0.4 eV.[29,30] The systematic study of Jacquemin and co-workers for solvated azobenzene shows that among a large amount of GGA, meta-GGA, conventional hybrids, and the recently developed range-separated hybrid functionals, the PBE0 and CAM-B3LYP functionals give a quantitative agreement on the spectroscopic state of some selected substituted azobenzenes.[19b] In combination with solvent via the PCM algorithm, mean absolute errors of 0.14 eV for CT in organic dyes, including azobenzene, have been obtained with the PBE0 functional.[19b] These results are even better that the ones obtained with range-separated hybrids. Recently, Tozer et al. have investigated the relationship between the excitation energy errors and the spatial overlap between the orbitals involved in the excitation, concluding that errors are large when the overlap is low.[38] In CT situations where no overlap between the involved orbitals in the CT state is observed, they strongly recommend the use of range-separated functionals, like the CAM-B3LYP functional.[39] In azobenzene and the herein studied HESAB dyes, the orbitals involved in the spectroscopic CT excitation should show a high-overlap due to conjugation over the rings (see Figure 2). In such cases, hydrid functionals with augmented amount of exact exchange, like PBE0, can deliver very accurate values because excitations with local character are also present, in agreement with ref 19b.

In the following, we shall investigate first the unsubstituted HESAB system using different protocols for reference. Table 4 collects the excitation energies, oscillator strengths, and the corresponding assignment of the most important peaks of the absorption spectra of the neutral and ionic HESAB model compounds (**1**/**1**$^-$) using RI-CC2, BP86, and PBE0 using different geometries, as specified. Figure 3a shows the experimental spectrum of **1** at pH = 3.52 and at pH = 11.08. At these pH values, the neutral (**1**) or the anionic (**1**$^-$) form is expected to be predominant, respectively, because the pK of **1** in methanol/buffer is 8.35 (in plain buffer, the pK_a is 7.64). Figure 3b−f displays the spectrum of **1** and **1**$^-$ at different levels of theory. In Figure 2, the corresponding frontier orbitals are displayed. As we can see, these are very similar for the neutral and ionic forms. The HOMO−1 of both anionic and neutral compounds **1**/**1**$^-$ corresponds to the n_N, the HOMO is a π orbital delocalized mainly in the azo moiety and the phenol moiety, and the LUMO orbital is the antibonding counterpart.

As in azobenzene, the lowest singlet excitation of **1** corresponds to a weak nπ^* state, followed by a strong $\pi\pi^*$ state. This is predicted by all of the computational approaches but the intensity of the nπ^* state is underestimated by all theories. In the following and for the sake of clarity, theoretical predictions will be denoted by eV_t (or nm_t) and experimental data by eV_e (nm_e).The most accurate RI-CC2/TZVP method (Figure 3b) obtain excitations at 2.85 eV_t (435 nm_t) and 3.82 eV_t (325 nm_t) for the S_1 (nπ^*) and S_2 ($\pi\pi^*$) states, respectively. The $\pi\pi^*$ state involves an electronic transition from the HOMO to the LUMO, that is, a CT from the azo-phenol moiety to the azo function (see Figure 2). The S_2 $\pi\pi^*$ state, measured at ca. 3.4 eV_e (360 nm_e), is overestimated with RI-CC2 by 0.4 eV probably due to the exclusion of the solvent. The use of a pure functional leads to a similar but opposite error: RI-BP86 predicts the S_2 $\pi\pi^*$ state at 3.07 eV_t, that is, underestimated by 0.4 eV with respect to the experiment (Table 4 and Figure 3c). This shift is reversed with the hybrid functional PBE0 (see Figure 3d), hence predicting a blue-shifted peak with an error of ca. 0.15 eV. The inclusion of solvent effects, only in the calculation of the excitation energies (Figure 3e) or both in the geometry and in the energies (Figure 3f), leads to values around 3.3 eV_t. The $\pi\pi^*$ state is then only blue-shifted with respect to the experiment by 0.1 eV. Because the differences in both latter procedures are not significant, the prescription PCM-PBE0//PBE0, that is, including the solvent only in the calculation of the energies but on vacuum geometries, seems to be a reasonable one to calculate the spectra of the substituted compounds.

The spectrum of **1**$^-$ is characterized by a strong band peaking at 2.7 eV_e (460 nm_e). This band corresponds to the $\pi\pi^*$ state, and depending on the computational approach, it is preceded, followed, or embedded into two low-lying very weak nπ^* transitions. With RI-CC2, the S_1 corresponds to the intense HOMO→LUMO $\pi\pi^*$ transition, calculated at 2.59 eV_t (479 nm_t) and therefore with an error of ca. 0.1 eV. The S_2 and S_3 are excitations from the n_O and n_N, respectively, to the LUMO, at 2.85 eV_t (435 nm_t) and 2.99 eV_t (415 nm_t). With RI-BP86, the S_3 at 2.68 eV_t (464 nm_t) is responsible for the intense $\pi\pi^*$ band, and the two nπ^* states are below, clearly underestimated with respect to the RI-CC2 values. Even if the RI-BP86 result for the $\pi\pi^*$ peak is in very close agreement with the experiment, one should keep in mind that solvent effects are not included, and hence this agreement is fortuitous. The use of the hybrid PBE0 functional intercalates the $\pi\pi^*$ state at 2.91 eV_t (426 nm_t) between the nπ^* states. When taking into account solvent effects without and with solvent during the optimizations (Figure 3e,f and Table 4), this transition is red-shifted, appearing at ca. 2.8 eV_t (∼440 nm_t), in reasonable agreement with the experimental absorption maximum.

The description of the nπ^* states deserves additional attention. It has been previously observed that typical global hybrids such as B3LYP or PBE0 show mean absolute errors similar to those of range-separated functionals, like CAM-B3LYP, in small organic dyes.[40] In solvated substituted azobenzenes, it has been shown that CAM-B3LYP outperforms other functionals, delivering minimum absolute errors as small as 0.02 eV for excitation energy of the nπ^* state.[32] Acceptable residual discrepancies (<0.2 eV) are obtained with the global hybrid PBE0 in the same

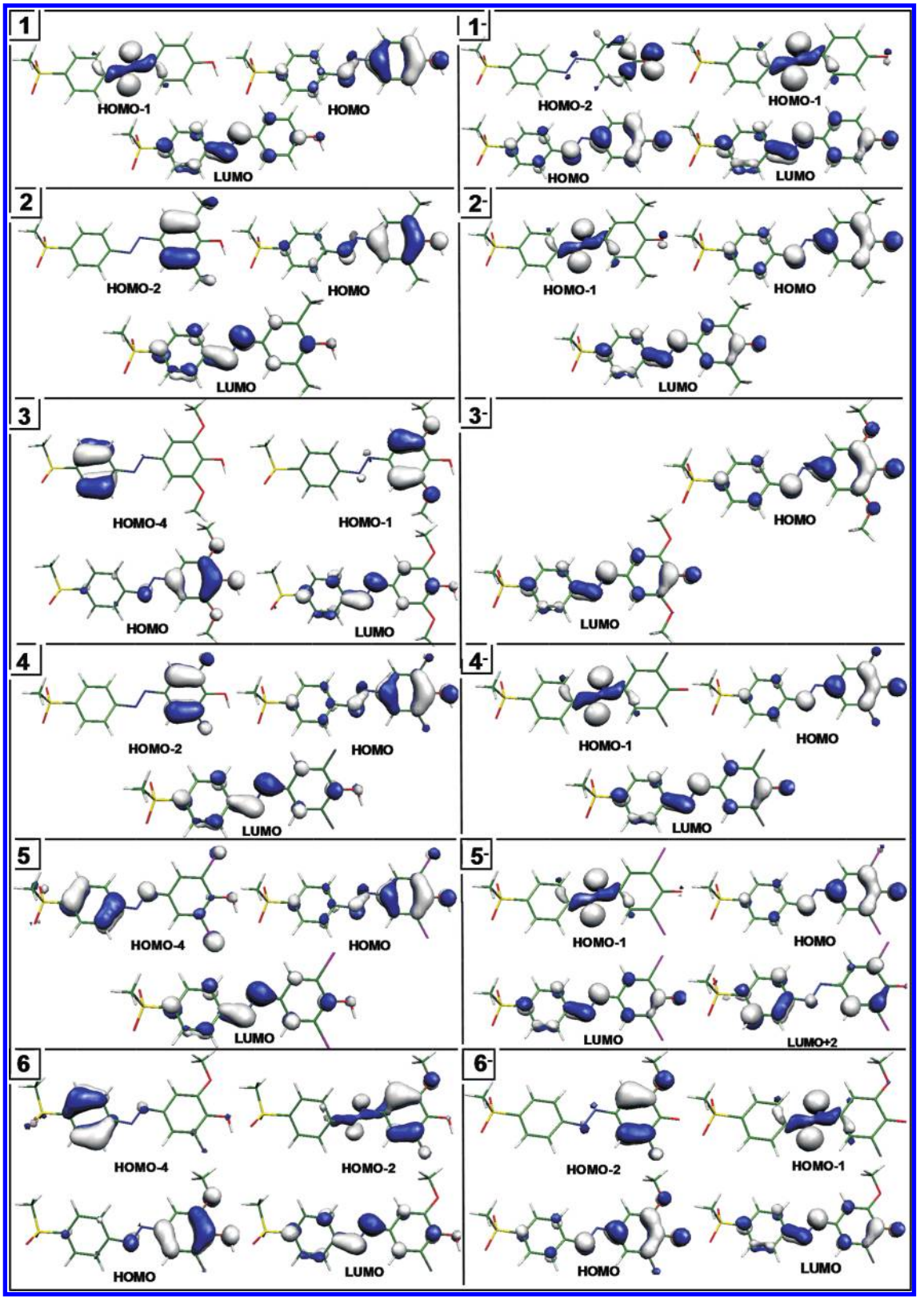

Figure 2. Kohn−Sham frontier orbitals involved in the main electronic transitions of $\mathbf{1}/\mathbf{1}^-$ to $\mathbf{6}/\mathbf{6}^-$ HESAB compounds.

compounds.[32] In our HESAB compound **1**, the nπ^* state is responsible for the less intense band centered at 2.72 eV_e (456 nm_e); see Table 2. It is likely that the nπ^* state in compound $\mathbf{1}^-$ is masked under the broad and intense $\pi\pi^*$ band; therefore, we shall limit our discussion to the energies of compound **1**. The best agreement for the nπ^* state is obtained with the accurate RI-

Table 4. Low-Lying Theoretical Electronic Transition Energies, ΔE (in eV and nm), with Oscillator Strengths, f, and Main Assignment (Configuration Interaction Coefficient) for Compounds 1 and Its Corresponding Anion 1^-

1					1^-				
	ΔE					ΔE			
state	eV	nm	f	assignment/c	state	eV	nm	f	assignment
		(RI-CC2//RI-BP86)					(RI-CC2//RI-BP86)		
S_1	2.85	435	0.017	$n_N-\pi^*$ (0.92)	S_1	2.59	479	1.100	$\pi-\pi^*$ (0.94)
S_2	3.82	325	0.999	$\pi-\pi^*$ (0.94)	S_2	2.85	435	0.098	$n_O-\pi^*$ (0.73)
					S_3	2.99	415	0.059	$n_N-\pi^*$ (0.79)
		(RI-BP86//RI-BP86)					(RI-BP86//RI-BP86)		
S_1	2.20	562	0.013	$n_N-\pi^*$ (0.94)	S_1	2.01	618	0.001	$n_O-\pi^*$ (0.95)
S_2	3.07	403	0.775	$\pi-\pi^*$ (0.92)	S_2	2.15	578	0.010	$n_N-\pi^*$ (0.94)
					S_3	2.68	464	1.100	$\pi-\pi^*$ (0.92)
		(PBE0//PBE0)					(PBE0/PBE0)		
S_1	2.62	473	0.012	$n_N-\pi^*$ (0.80)	S_1	2.65	468	0.086	$n_N-\pi^*$ (0.57)
S_2	3.59	345	0.922	$\pi-\pi^*$ (0.79)	S_2	2.91	426	1.210	$\pi-\pi^*$ (0.51)
					S_3	3.05	406	0.008	$n_O-\pi^*$ (0.68)
		(PCM-PBE0//PBE0)					(PCM-PBE0//PBE0)		
S_1	2.62	473	0.032	$n_N-\pi^*$ (0.62)	S_1	2.66	465	0.318	$n_N-\pi^*$ (0.57)
S_2	3.29	377	1.027	$\pi-\pi^*$ (0.60)	S_2	2.85	435	1.062	$\pi-\pi^*$ (0.51)
					S_3	3.59	345	0.000	$n_O-\pi^*$ (0.68)
		(PCM-PBE0//PCM-PBE0)					(PCM-PBE0//PCM-PBE0)		
S_1	2.62	473	0.006	$n_N-\pi^*$ (0.65)	S_1	2.71	457	0.002	$n_N-\pi^*$ (0.66)
S_2	3.35	370	1.056	$\pi-\pi^*$ (0.67)	S_2	2.82	439	1.318	$\pi-\pi^*$ (0.51)
					S_3	3.58	346	0.000	$n_O-\pi^*$ (0.68)

CC2 method (2.85 eV_t) and with the global hybrid PBE0 functional (2.62 eV_t). The inclusion of solvent effects on the calculation of the vertical excitations and on the optimized geometries has no effect on the energy of the nπ^* excitation (see Table 4). This negligible effect is in agreement with the small shifts that have been observed for other substituted azobenzene dyes when comparing gas-phase and solvated results.[30] The intensities of the nπ^* bands, however, are different depending on the protocol. The oscillator strengths of the nπ^* states of compounds **1** and $\mathbf{1}^-$ are higher with PCM-PBE0//PBE0 than with the PBE0/PBE0 model or PCM-PBE0//PCM-PBE0 (see Table 4), and hence PCM-PBE0//PBE0 reproduces best the experimental evidence (see Figure 3e). As a consequence a broader $\pi\pi^*$ band for compound $\mathbf{1}^-$ is observed with the PCM-PBE0//PBE0 protocol than with the other approaches (compare Figure 3e with d and f). The increase of nπ^* intensity is due to electrostatic effects, because, for instance, the mixing of the nπ^* with the $\pi\pi^*$ state for compound $\mathbf{1}^-$ is the same with PCM-PBE0//PBE0 and PBE0//PBE0, and thus an increased absorption due to mixing with the strong $\pi\pi^*$ excitation can be ruled out (see wave function coefficients of S_1 in Table 4). A more likely explanation roots to the geometry of the compounds. As we stated above, when considering bulk solvent effects on the optimization of the geometries, slightly more planar optimized structures are obtained. This planarization affects strongly the intensity of the nπ^* states of **1** and $\mathbf{1}^-$ (compare exemplarily the S_1 oscillator strength values of $\mathbf{1}^-$ with the PCM-PBE0//PBE0 and PCM-PBE0//PCM-PBE0 theoretical models). For the latter procedure, a purer nπ^* state is obtained, which might contribute to the enormous decreasing of the intensity. Focusing only on the intensities of the nπ^* state, it is surprising that the agreement with the experiment is better with PCM-PBE0//PBE0 rather than with the PCM-PBE0//PCM-PBE0 model. A plausible explanation for this fact might be the flat nature of the potential energy surface in the vicinity of the planarization region, as suggested by the geometric controversy with the different theoretical approaches. To address this geometrical effect and its consequent effects on the intensities of the nπ^* state, molecular dynamic simulations evaluating the temperature effects on the UV/vis electronic spectrum might be appropriate, as has been done in *trans*-stilbene.[41]

Summarizing, the experimental spectra (Figure 3a) agree reasonably well with those obtained with PCM-PBE0/PBE0 (Figure 3e). The main band of **1** is theoretically blue-shifted by ca. 15 nm, and the one of $\mathbf{1}^-$ is red-shifted by 25 nm (see Table 4). Yet, it is fair to mention that the theoretical peaks of **1** and $\mathbf{1}^-$ at 377 and 435 nm_t agree much better with the peaks obtained in pure methanol at 364 and 441 nm_e (see Table 3). Therefore, we can infer that the differences between theory and experiment are mainly due to the fact that while the experimental data in Table 4 and Figure 3 are obtained in a buffered 1:1 water/methanol solutions, theory considers only pure methanol as a solvent.

As a general remark, we can conclude that in both the experimental and the theoretical spectra, a strong red (bathochromic) shift can be observed in the band of the anionic form of the dye with respect to the neutral form. This shift can be easily rationalized looking at the responsible transitions in both neutral and anionic forms (cf., Table 4). The involved orbitals, the HOMO/LUMO of the neutral and the anion, exhibit a similar conjugated π character but a different electronic redistribution (Figure 2). Thus, the bands in **1** and $\mathbf{1}^-$ have origin in frontier orbitals of similar character but with different energies. Because of additional electrostatic repulsion with the negative charge in $\mathbf{1}^-$, all occupied orbitals are shifted to higher energies, leading to smaller occupied-virtual gaps with respect to **1**, and therefore red-shifted peaks are obtained for the HOMO→LUMO $\pi\pi^*$ transitions. This is responsible for the

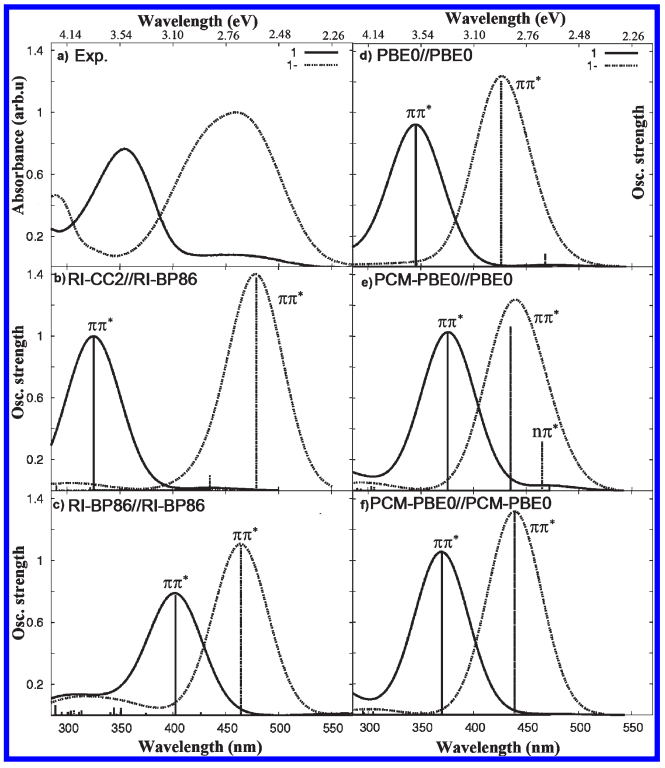

Figure 3. UV−vis absorption spectra of **1** (solid) and $\mathbf{1}^-$ (dashed). (a) Experimental spectrum normalized to 1 in arbitrary units, (b) RI-CC2//RI-PB86, (c) RI-BP86//RI-BP86, (d) PBE0//PBE0, (e) PCM-PBE0//PBE0, and (f) PCM-PBE0//PCM-PBE0. The theoretical spectra are convoluted with a Lorentzian function with a full width at half-maximum (fwhm) of 60 nm; the corresponding transitions are marked with vertical lines.

different color of both forms (neutral and anionic) and consequently allows for this compound being used as an indicator (see Table 2).

To conclude, because the spectroscopic states ($\pi\pi^*$), as well as the nπ^* states of the pair $\mathbf{1}/\mathbf{1}^-$ are well described with the PCM-PBE0/PBE0 model, this level of theory will be employed to study the HESAB compounds $\mathbf{2}/\mathbf{2}^- - \mathbf{6}/\mathbf{6}^-$.

Substitution Effects in the UV−Vis Spectra. Having analyzed the basic spectral properties of the neutral and anionic forms of the reference compound **1** with respect to the bare azobenzene, we now proceed to evaluate how the electronic transitions are modulated by substitution on the phenol moiety. The corresponding spectra for the HESAB species with electron donor ($\mathbf{2}/\mathbf{2}^-$ and $\mathbf{3}/\mathbf{3}^-$), electron acceptor ($\mathbf{4}/\mathbf{4}^-$ and $\mathbf{5}/\mathbf{5}^-$), and both electron-donor and electron-acceptor ($\mathbf{6}/\mathbf{6}^-$) substituents are shown in Figure 4. The main electronic transitions are collected in Table 5, and selected orbitals are found in Figure 2.

As stated above, the substituents influences not only the pK_a value[16] but also the spectral properties, altering the isosbestic point that appears between both anionic and neutral forms in the UV−vis spectrum, and in turn determining to which extent these compounds can be used as indicators. Even if both methyl and methoxy groups donate charge to the aromatic ring, the spectra of $\mathbf{2}/\mathbf{2}^-$ and $\mathbf{3}/\mathbf{3}^-$ are different (compare Figure 4a and b). The maximum absorption peaks of $\mathbf{2}/\mathbf{2}^-$ are separated by 126 nm$_e$, while this gap is considerably reduced in the pair $\mathbf{3}/\mathbf{3}^-$, showing partially overlapping bands and an isosbestic point less defined. The main changes are in the spectra of **2** and **3**, while the spectra of $\mathbf{2}^-$ and $\mathbf{3}^-$ are only shifted by 26 nm$_e$. In the dimethyl compound (**2**), the bright S_2 state located at 374 nm$_t$ corresponds to an HOMO→LUMO $\pi\pi^*$ excitation from the azo and phenol moieties to the π^* orbital, this transition being analogous to the one found in **1**. Additionally, a less intense $\pi\pi^*$ transition contributes to the tail of the band at higher energies (S_3 state, see Table 5). In the dimethoxy compound (**3**), on the other hand, at least two $\pi\pi^*$ states (S_2 and S_3) contribute to the broad band peaking at 460 nm$_e$. Presumably the wide profile of the band is due to the S_3 state, which theoretically is determined at 362 nm$_t$. An additional intense transition corresponding to the S_5 contributes to the near-UV spectrum; this is an HOMO−4→LUMO excitation from a π orbital localized in the phenyl moiety to π^*_{azo} (see Figure 2). Note that in the case of **3** there is a stabilization of the n_N orbital (HOMO−2). This different behavior obeys the electronic effects: the methoxy group is more electron-donating than the methyl group and hence destabilizes to a major extent the localized and delocalized π orbitals, HOMO−1 and HOMO, respectively, of **3**. Accordingly, these orbitals correspond to HOMO−2 and HOMO, in compound **2**. Consequently, the HOMO→LUMO, $\pi\pi^*_{azo}$, transition at 403 nm$_t$ is red-shifted with respect to **2** (compare with 374 nm$_t$ in **2**).

The agreement between the experimental and theoretical spectra for the pairs $\mathbf{2}/\mathbf{2}^-$ and $\mathbf{3}/\mathbf{3}^-$ is reasonable, with general blue-shifts from theory to experiment (Figure 4). The spectrum of **2** is simpler and similar to that of the unsubstituted compound **1**. Likewise, the spectra of the anionic compounds ($\mathbf{2}^-$ and $\mathbf{3}^-$) resemble the spectra of $\mathbf{1}^-$. They are both characterized by a strong peak, experimentally located at 499 and 525 nm$_e$, and theoretically blue-shifted at 456 nm$_t$ and 484 nm$_t$, respectively. In $\mathbf{2}^-$, both S_1 and S_2 states contribute almost equally to the main band, which then can be assigned as a mixture of the $\pi\pi^*_{azo}$ and $n\pi^*_{azo}$ electronic excitations (Table 4). On the contrary, in compound $\mathbf{3}^-$, this peak is due to the S_1 state, which is a HOMO→LUMO transition, localized in the $\pi\pi^*_{azo}$ orbitals, as in $\mathbf{1}^-$.

The nπ^* transitions in $\mathbf{2}/\mathbf{2}^-$ and $\mathbf{3}/\mathbf{3}^-$ are very similar to those encountered in the unsubstituted pair $\mathbf{1}/\mathbf{1}^-$ and show similar trends in terms of oscillator strengths (rather small in **2**, **3**, and $\mathbf{3}^-$). As in the pair $\mathbf{1}/\mathbf{1}^-$, the nπ^* transitions are red-shifted upon deprotonation. These effects will also appear in the electron-withdrawing substituted compounds (vide infra). Experimentally, the band of **2** shows a shoulder centered at 427 nm$_e$, which is most likely due to the nπ^* transition (466 nm$_t$). The intensity of this transition is theoretically underestimated. Interestingly, in $\mathbf{2}^-$, where the nπ^* transition is mixed with the $\pi\pi^*$ transition (recall S_1 and S_2 in Table 5), higher oscillator strengths are obtained due to this mixing. To investigate whether this mixing changes when solvent effects are included in the optimization, which redounds in a more planar geometry (vide supra), and whether energies can be improved, test calculations in $\mathbf{2}^-$ have been performed with the PCM-PBE0//PCM-PBE0 approach. The resulting energies and oscillator strengths are also included in Table 5 in brackets. As we can see, the mixing between the nπ^* and $\pi\pi^*$ transitions is slightly reduced (as we saw in the pair $\mathbf{1}/\mathbf{1}^-$), rendering different oscillator strengths: a smaller/larger value for the S_1/S_2 states, respectively. However, the solvent effect does not improve substantially the energies, although a slight shift toward the experimental values is obtained.

The neutral forms **4** and **5** show a broad band peaking at 355 and 354 nm$_e$, respectively (cf., Table 2). As in the previous cases,

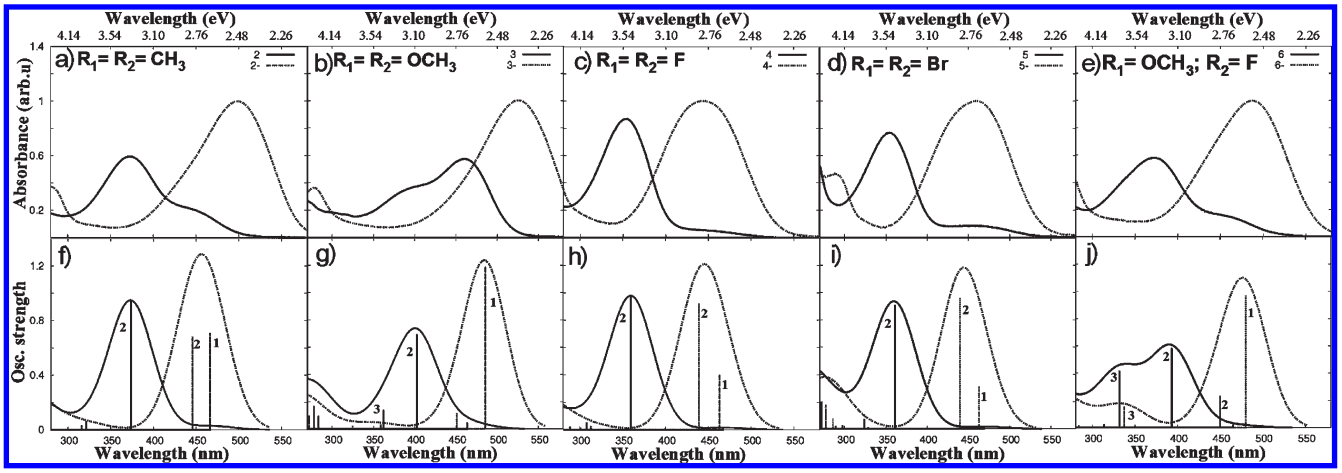

Figure 4. Experimental (top) and PCM-PBE0//PBE0 (bottom) spectra of neutral (solid) and anionic (dashed) compounds. The theoretical spectra are convoluted with a Lorentzian function with a full width at half-maximum (fwhm) of 60 nm; the transitions are marked with vertical lines indicating the corresponding singlet excited state.

Table 5. PCM-PBE0//PBE0 Calculated Electronic Excited States of Compounds 2−6 and Corresponding Anions[a]

state	ΔE	f	assignment	state	ΔE	f	assignment
		2				**2**$^-$	
S_1	2.66(466)	0.029	H-1→L (0.62) $n_N-\pi^*$	S_1	2.66(466) [2.71(457)][b]	0.709 [0.357]	H-1→L (−0.45) $n_N-\pi^*$ H→L (0.45) $\pi-\pi^*$ [H-1→L (0.57) $n_N-\pi^*$] [H→L (−0.31) $\pi-\pi^*$]
S_2	3.32(374)	0.940	H→L (0.61) $\pi-\pi^*$	S_2	2.78(446) [2.73(454)][b]	0.684 [0.988]	H-1→L (0.49) $n_N-\pi^*$ H→L (0.41) $\pi-\pi^*$ [H-1→L (0.34) $n_N-\pi^*$] [H→L (0.52) $\pi-\pi^*$]
S_3	3.86(321)	0.063	H-2→L (0.68) $\pi-\pi^*$	S_4	3.86(321) [3.83(324)][b]	0.023 [0.025]	H-3→L (0.68) $\pi-\pi^*$ [H-3→L (0.68) $\pi-\pi^*$]
		3				**3**$^-$	
S_1	2.67(464)	0.048	H-2→L (0.61) $n_N-\pi^*$	S_1	2.55(486)	1.190	H→L (0.57) $\pi-\pi^*$
S_2	3.08(403)	0.694	H→L (0.61) $\pi-\pi^*$	S_2	2.75(451)	0.115	H-1→L (0.65) $n_N-\pi^*$
S_3	3.42(362)	0.138	H-1→L (0.64) $\pi-\pi^*$	S_3	3.46(359)	0.035	H-2→L (0.68) $\pi-\pi^*$
S_5	4.47(278)	0.168	H-4→L(0.48) $\pi-\pi^*$				
		4				**4**$^-$	
S_1	2.65(467)	0.016	H-1→L (0.63) $n_N-\pi^*$	S_1	2.68(463)	0.404	H-1→L (0.54) $n_N-\pi^*$
S_2	3.45(360)	0.972	H→L (0.62) $\pi-\pi^*$	S_2	2.82(439)	0.921	H→L (0.49) $\pi-\pi^*$
S_3	4.03(308)	0.052	H-2→L (0.68) $\pi-\pi^*$	S_4	3.97(313)	0.024	H-2→L (0.68) $\pi-\pi^*$
		5				**5**$^-$	
S_1	2.64(469)	0.016	H-1→L (0.62) $n_N-\pi^*$	S_1	2.68(463)	0.314	H-1→L (0.57) $n_N-\pi^*$
S_2	3.44(361)	0.909	H→L (0.62) $\pi-\pi^*$	S_2	2.82(440)	0.959	H→L (0.53) $\pi-\pi^*$
S_3	3.83(324)	0.072	H-2→L (0.67) $\pi-\pi^*$	S_5	4.17(297)	0.027	H→L+1 (0.63) $\pi-\pi^*$
S_5	4.57(271)	0.198	H-4→L (0.65) $\pi-\pi^*$	S_6	4.34(286)	0.075	H→L+2 (0.58) $\pi-\pi^*$
		6				**6**$^-$	
S_1	2.67(465)	0.022	H-1→L (0.58) $n_N-\pi^*$	S_1	2.58(480)	0.973	H→L (0.55) $\pi-\pi^*$
S_2	3.15(393)	0.583	H→L(0.63) $\pi-\pi^*$	S_2	2.75(450)	0.232	H-1→L (0.61) $n_N-\pi^*$
S_3	3.73(332)	0.418	H-2→L (0.61) $\pi-\pi^*$	S_3	3.67(337)	0.154	H-2→L (0.67) $\pi-\pi^*$
S_5	4.56(271)	0.116	H-4→L (0.47) $\pi-\pi^*$	S_5	3.95(314)	0.028	H→L+1 (0.66) $\pi-\pi^*$

[a] The transitions energies, ΔE, for the most relevant transitions are given in eV (nm) with oscillator strengths, f, and main assignments (configuration interaction coefficient). [b] Values in brackets obtained at the PCM-PBE0//PCM-PBE0 level of theory.

the transitions underlying these bands are the HOMO→LUMO transitions of $\pi\pi^*$ character. In **4**, this band is assigned to the bright S_2 state, located at 360 nm_b in excellent agreement with the experiment. In **5**, not only the S_2 (361 nm_t) but to a minor extent the much weaker S_3 (324 nm_t) state contributes to this band. In both compounds, the S_2 state is an HOMO→LUMO transition with $\pi\pi^*_{azo}$ character. In **5**, the S_3 state is an excitation from the HOMO−2, that is, a π orbital localized on the phenol moiety but not on the azo moiety. As it can be seen, the S_2 transition in the electron-withdrawing compounds is blue-shifted

dx.doi.org/10.1021/ct1007235 |J. Chem. Theory Comput. 2011, 7, 1062–1072

Table 6. Experimental and PCM-PBE0//PBE0 Calculated Ratios between the Heights of the Anion and Neutral Main Bands of Compounds 1−6 and 1^-−6^-, as well as the Ratio between the Calculated Oscillator Strengths *f* of the Main $\pi\pi^*$ Transitions Underlying the Main Band of the Spectra

	$1^-/1$	$2^-/2$	$3^-/3$	$4^-/4$	$5^-/5$	$6^-/6$
experimental	1.30	1.68	1.74	1.14	1.30	1.72
theoretical	1.21	1.36	1.67	1.24	1.26	1.80
$f^-(\pi\pi^*)/f(\pi\pi^*)$	1.04	1.48[a]	1.71	0.95	1.06	1.67[b]

[a] Obtained considering the sum of the oscillator strengths of S_1 and S_2 of $\mathbf{2}^-$, because the $\pi\pi^*$ and $n\pi^*$ are strongly mixed (see Table 5). [b] Obtained considering only the oscillator strength of S_2 of **6**.

both theoretically and experimentally in comparison to its analogous S_2 in the electron-donating compounds (**2**, **3**) and the unsubstituted compound **1** (Table 5). This blue-shift can be attributed to the stabilization/destabilization of the HOMO/LUMO pair of orbitals due to electronic effects. Also well represented is the onset of the second band observed in the spectrum of **5** (Figure 4d), which can be assigned to the S_5 state, located at 271 nm_t, and corresponds to an excitation from a π orbital localized on the phenyl ring (HOMO−4, in Figure 2) to the π^*_{azo} orbital.

As with the electron donor derivatives ($\mathbf{2}^-$ and $\mathbf{3}^-$) and the bare compound $\mathbf{1}^-$, the HOMO→LUMO transition is responsible for the electronic properties of $\mathbf{4}^-$ and $\mathbf{5}^-$. Small blue-shifts are observed with respect to $\mathbf{1}^-$. As it was found in the other HESAB compounds, the red-shifted bands of $\mathbf{4}^-$ and $\mathbf{5}^-$ are more intense than the corresponding neutral ones. We note that the theoretical values are very close to the experimental ones: the theoretical absorption maxima in $\mathbf{5}^-$ are blue-shifted ca. 12 nm_t and in $\mathbf{4}^-$ ca. 1 nm_t, with respect to the experiment (cf., Table 3). The main band of $\mathbf{5}^-$, peaking at 460 nm_e, is explained by the S_1 and S_2 states, which correspond to the $n\pi^*_{azo}$ and a $\pi\pi^*$ transition, respectively (see Table 5). Additionally, compound $\mathbf{5}^-$ also shows a weaker band at higher energies (292 nm_e), which is theoretically well described by the S_5 and S_6 $\pi\pi^*$ states (297 and 286 nm_t). It is gratifying to see that in most of the cases, the deviation from the experiment is below 0.1 eV. The maximum discrepancy between theory and experiment is found in the description of the main band of **3**, with an error accounting to ca. 0.35 eV. These errors are in the upper limit of accuracy that can be expected for this methodology.

In summary, when comparing the spectroscopic properties of electron-donor and electron-withdrawing substituted HESABs with $\mathbf{1}/\mathbf{1}^-$, we can state the following: First, there is a significant red-shift of the main peaks of the anionic forms of the electron-donor compounds with respect to $\mathbf{1}^-$ (compare 460 nm_e in $\mathbf{1}^-$ with 499 and 525 nm_e in $\mathbf{2}^-$ and $\mathbf{3}^-$, respectively, in Table 2) due to electronic effects, and although less striking, a small red-shift is present in the main peak of the acid forms (see 361 nm_e in **1** versus 373 and 460 nm_e in **2** and **3**). In electron-withdrawing compounds, the trend is inverse; that is, the absorption of the basic forms is slightly blue-shifted in comparison to $\mathbf{1}^-$ (compare 460 nm_e in $\mathbf{1}^-$ with 444 and 460 nm_e in $\mathbf{4}^-$ and $\mathbf{5}^-$). The main peaks of the acid forms are also slightly blue-shifted (see Table 2). Despite being small, these differences are recovered by the DFT calculations.

The spectra of the fluoromethoxy pair $\mathbf{6}/\mathbf{6}^-$ (Figure 4e,j) resemble those of $\mathbf{1}/\mathbf{1}^-$ due to compensating electronic effects. The peak of **6** located at 374 nm_e can be assigned to the S_2 and S_3 states, located at 393 and 332 nm_t. The S_2 state corresponds to the usual HOMO→LUMO transition of $\pi\pi^*_{azo}$ character. The S_3 is also a $\pi\pi^*$ transition, but starts from the HOMO−2 orbital, which is mainly located in the phenol moiety (see Figure 2), as it has been found in **1**, **2**, and **4**. The spectrum of $\mathbf{6}^-$ peaks at 487 nm_e and it can be described by the S_1 (480 nm_t), which is the $\pi\pi^*_{azo}$ transition and a non-negligible contribution of the S_2 $n\pi^*_{azo}$ state.

Finally, we have considered it of interest to analyze the effect of the pH and substitution pattern on the relative transition intensities. In Table 6, we have calculated the ratio between the heights of the anion and neutral main bands, using the experimental and computed PCM-PBE0//PBE0 spectra. The experimental values show that electron-donor species increases this ratio, while electron-withdrawing groups leave this value almost unchanged. It is gratifying to see that these trends are also theoretically reproduced. Additionally, we have calculated the ratio between the calculated oscillator strengths *f* of the strong $\pi\pi^*$ transitions underlying the peaks of the anion and neutral spectra. The comparison of these ratios indicates the differences in intensity with respect to the reference pair $\mathbf{1}/\mathbf{1}^-$. As we can see, the trends for electron-donor ($\mathbf{2}/\mathbf{2}^-$ and $\mathbf{3}/\mathbf{3}^-$) and electron-withdrawing ($\mathbf{4}/\mathbf{4}^-$ and $\mathbf{5}/\mathbf{5}^-$) substitution are maintained. The value obtained for the compounds $\mathbf{6}/\mathbf{6}^-$ is not really instructive because the spectrum is broad due to several transitions, but for the sake of uniformity only one transition (S_2) has been taken into account.

5. CONCLUSIONS

In the present Article, the absorption spectra of substituted 2-hydroxyethylsulfonyl azobenzene (HESAB) pH indicator dyes are reported and theoretically assigned with the help of quantum chemical calculations. HESAB indicator dyes can be used for optically monitoring pH in the range from 3 to 10 and can be covalently linked to sensor layers exhibiting high chemical stability, as we have recently reported.[16] HESAB chemistry is not just limited to absorbance spectroscopy but could also be used to develop emission dyes. The absorbance spectra of all the neutral and anionic counterparts are well separated; accordingly, the color changes of HESAB dyes in going from acid to base form (i.e protonated to deprotonated form) are from yellow to orange or red, hence making feasible its use as pH indicator dyes. Substitution of HESAB complexes by electron-donor and electron-withdrawing moieties biases not only the pK_a values but also the spectroscopic properties of HESAB complexes. The differences of the spectroscopic features upon substitution as well as between the anionic and neutral forms (measured under different pH conditions) have been theoretically elucidated. The good agreement between theory and experiment has been achieved using the density functional protocol PCM-PBE0/PBE0, which includes the solvent effect in the energies with a continuum model but geometries optimized in gas phase. With this theoretical model, deviation from the experiment in the description of the $n\pi^*$ and $\pi\pi^*$ states is below 0.1 eV. Inclusion of additional solvent effects in the optimization of the geometries leads to minor improvements on the transition energies. However, because the geometries optimized in the presence of solvent are more planar than those in gas phase, the intensities of the $n\pi^*$ transitions decrease substantially in comparison to that obtained in gas phase. In the species studied here, this effect leads to a

worse agreement with the weak experimental nπ^* bands, very likely because temperature effects prevent the molecule from remaining planar, as indicated by the low frequency modes corresponding to the out-of-plane motion of the rings. Whether inclusion of solvent effects in the geometries is necessary in other cases needs to be cautiously evaluated for each particular case.

In general, from this study, the following conclusions are extracted for the HESAB dyes:

(i) The spectroscopic state of all of the neutral and anionic HESAB dyes here investigated is the $\pi\pi^*$ transition. This is then the state that determines the functionality of these complexes as pH indicators, while the nπ^* transitions are much weaker or even dark.

(ii) In all of the HESAB dyes, a red-shift is observed upon deprotonation. This effect can be trivially explained in terms of the additional electrostatic repulsion between the negative charge and the occupied orbitals, which are then shifted to higher energies, thus leading to smaller occupied-virtual gaps.

(iii) In the electron-donor compounds, both the neutral and the anionic forms show peaks red-shifted with respect to the unsubstituted compound. An inverse trend is observed in the studied electron-withdrawing derivatives; peaks are blue-shifted with respect to the unsubstituted compound. These effects have been rationalized theoretically in terms of the stabilization/destabilization of the orbital levels due to electronic effects upon substitution. The consequences of substitution on the optical properties of the pH indicators are translated in a change of the color pattern between the pair of complexes, for instance, going from pale yellow to orange in $\mathbf{1}/\mathbf{1}^-$ and from yellow/orange to red in $\mathbf{3}/\mathbf{3}^-$.

(iv) In the compound where both electron-donor and -withdrawing substituents are present, the spectrum resembles very much that of the unsubstituted HESAB, due to compensating electronic effects.

When planning the synthesis of new indicator dyes, one important issue is the possible prediction of their future optical properties. This is important when sensor dyes have to be made spectrally compatible with cheap light sources (e.g., light emitting diodes or laser diodes). Furthermore, well-separated absorbance spectra between acid and base form simplify the setup of the optical sensor device and enhance the signal-to-noise ratio. In the present work, a good correlation between calculated and experimental absorbance spectra has been achieved, thus paving the way for the dedicated design of new sensor dyes and sensor devices.

AUTHOR INFORMATION

Corresponding Author

*Fax: +49 3641 948302. E-mail: leticia.gonzalez@uni-jena.de.

ACKNOWLEDGMENT

This work has been funded by the Carl-Zeiss foundation (D.E.), the BMBF project "Aquaoptrode" (no. 13N9535), the projects MO 1062/5-1 and MO 1062/6-1 of the Deutsche Forschungsgemeinschaft, and the project AZ-Nr.: 20.10-3410-2 (Projekt Sensormaterialien) of the Bayerische Staatsministerium für Wirtschaft, Infrastruktur, Verkehr und Technologie. Computer time in the Rechnenzentrum of the Friedrich-Schiller-Universität Jena is gratefully acknowledged.

REFERENCES

(1) McMillan, G. K.; Cameron, R. A. *Advanced pH Measurement and Control*, 3rd ed.; ISA: Research Triangle Park, NC, 2004.

(2) See, for example: (a) Orellana, G., Moreno-Bondi, M. C., Eds. *Springer Series on Chemical Sensors and Biosensors*; Springer-Verlag: Berlin, Germany, 2004; Vol. 1. (b) Narayanaswamy, R., Wolfbeis, O. S., Eds. *Optical Sensors: Industrial, Enviromental and Diagnostic Applications*; Springer: Berlin, Heidelberg, 2004. (c) Wolfbeis, O. S. *Anal. Chem.* **2006**, *78*, 3859.

(3) Trupp, S.; Alberti, M.; Carofiglio, T.; Lubian, E.; Lehmann, H.; Heuermann, R.; Yacoub-George, E.; Bock, K.; Mohr, G. J. *Sens. Actuators, B* **2010**, *150*, 206.

(4) (a) Durr, H.; Bouas-Laurent, H. *Photochromism, Molecules and Systems*; Elsevier: Amsterdam, 1990. (b) Barrett, C. J.; Mamiya, J.; Yager, K. G.; Ikeda, T. *Soft Matter* **2007**, *3*, 1249.

(5) See, for example: Feringa, B. L. *Molecular Switches*; Wiley-VCH: Germany, 2003.

(6) Shinkai, S.; Manabe, O. *Top. Curr. Chem.* **1984**, *121*, 76.

(7) Hugel, T.; Holland, N. B.; Cattani, A.; Moroder, L.; Seitz, M.; Gaub, H. E. *Science* **2002**, *296*, 1103.

(8) Natansohn, A.; Rochon, P. *Chem. Rev.* **2002**, *102*, 4139.

(9) Spörlein, S.; Carstens, H.; Satzger, H.; Renner, C.; Behrendt, R.; Moroder, L.; Tavan, P.; Zinth, W.; Wachtveitl, J. *Proc. Natl. Acad. Sci. U. S.A.* **2002**, *99*, 7998.

(10) Carofiglio, T.; Fregonese, C.; Mohr, G. J.; Rastrelli, F.; Tonellato, U. *Tetrahedron* **2006**, *62*, 1502.

(11) Mohr, G. J. *Anal. Chim. Acta* **2004**, *508*, 233.

(12) Mohr, G. J. *Dyes Pigm.* **2004**, *62*, 77.

(13) Mohr, G. J. *Sens. Actuators, B* **2003**, *90*, 31.

(14) Ward, C. J.; Patel, P.; James, T. D. *J. Chem. Soc., Perkin Trans.* **2002**, *1*, 462.

(15) Mohr, G. J. *Chem. Commun.* **2002**, *22*, 2646.

(16) Mohr, G. J.; Müller, H.; Bussemer, B.; Stark, A.; Carofiglio, T.; Trupp, S.; Heuermann, R.; Henkel, T.; Escudero, D.; González, L. *Anal. Bioanal. Chem.* **2008**, *392*, 1411.

(17) (a) Runge, E.; Gross, E. K. U. *Phys. Rev. Lett.* **1984**, *52*, 997. (b) Stratmann, R. E.; Scuseria, G. E.; Frisch, M. J. *J. Chem. Phys.* **1998**, *109*, 8218. (c) Casida, M. E. In *Time-Dependent Density-Functional Response Theory for Molecules*; Chong, D. P., Ed.; World Scientific: Singapore, 1995; Vol. 1, pp 155−192. (d) Koch, W.; Holthausen, M. C. *A Chemist's Guide to Density Functional Theory*; Wiley-VCH: Germany, 2000. (e) Barone, V.; Polimeno, A. *Chem. Soc. Rev.* **2007**, *36*, 1724. (f) Jacquemin, D.; Perpète, E. A.; Ciofini, I.; Adamo, C. *Acc. Chem. Res.* **2009**, *42*, 326.

(18) See, for example: (a) Goerigk, L.; Moellmann, J.; Grimme, S. *Phys. Chem. Chem. Phys.* **2009**, *11*, 4611. (b) Goerigk, L.; Grimme, S. *J. Chem. Phys.* **2010**, *132*, 1841103. (c) Jacquemin, D.; Perpète, E. A.; Ciofini, I.; Adamo, C. *J. Chem. Theory Comput.* **2010**, *6*, 1532.

(19) (a) Jacquemin, D.; Preat, P.; Wathelet, V.; Fontaine, M.; Perpète, E. A. *J. Am. Chem. Soc.* **2006**, *128*, 2072. (b) Jacquemin, D.; Perpète, E. A.; Scuseria, G. E.; Ciofini, I.; Adamo, C. *J. Chem. Theory Comput.* **2008**, *4*, 123.

(20) Adamo, C.; Barone, V. *J. Chem. Phys.* **1999**, *110*, 6158.

(21) (a) Cossi, M.; Barone, V.; Mennucci, B.; Tomasi, J. *Chem. Phys. Lett.* **1998**, *286*, 253. (b) Mennucci, B.; Tomasi, J. *J. Chem. Phys.* **1997**, *106*, 5151.

(22) Christiansen, O.; Koch, H.; Jørgensen, P. *Chem. Phys. Lett.* **1995**, *243*, 409.

(23) Hättig, C.; Weigend, F. *J. Chem. Phys.* **1995**, *243*, 409.

(24) Becke, A. D. *Phys. Rev. A* **1998**, *38*, 3098.

(25) Perdew, J. P. *Phys. Rev. B* **1986**, *33*, 8822.

(26) Ahlrichs, R.; Bär, M.; Häser, M.; Horn, H.; Kölmel, C. *Chem. Phys. Lett.* **1989**, *162*, 165.

(27) Frisch, M. J.; Trucks, G. W.; Schlegel, H. B.; Scuseria, G. E.; Robb, M. A.; Cheeseman, J. R.; Montgomery, J. A., Jr.; Vreven, T.; Kudin, K. N.; Burant, J. C.; Millam, J. M.; Iyengar, S. S.; Tomasi, J.; Barone, V.; Mennucci, B.; Cossi, M.; Scalmani, G.; Rega, N.; Petersson, G. A.; Nakatsuji, H.; Hada, M.; Ehara, M.; Toyota, K.; Fukuda, R.; Hasegawa, J.; Ishida, M.; Nakajima, T.; Honda, Y.; Kitao, O.; Nakai, H.; Klene, M.; Li, X.; Knox, J. E.; Hratchian, H. P.; Cross, J. B.; Bakken, V.; Adamo, C.; Jaramillo, J.; Gomperts, R.; Stratmann, R. E.; Yazyev, O.; Austin, A. J.; Cammi, R.; Pomelli, C.; Ochterski, J. W.; Ayala, P. Y.; Morokuma, K.; Voth, G. A.; Salvador, P.; Dannenberg, J. J.; Zakrzewski, V. G.; Dapprich, S.; Daniels, A. D.; Strain, M. C.; Farkas, O.; Malick, D. K.; Rabuck, A. D.; Raghavachari, K.; Foresman, J. B.; Ortiz, J. V.; Cui, Q.; Baboul, A. G.; Clifford, S.; Cioslowski, J.; Stefanov, B. B.; Liu, G.; Liashenko, A.; Piskorz, P.; Komaromi, I.; Martin, R. L.; Fox, D. J.; Keith, T.; Al-Laham, M. A.; Peng, C. Y.; Nanayakkara, A.; Challacombe, M.; Gill, P. M. W.; Johnson, B.; Chen, W.; Wong, M. W.; Gonzalez, C.; Pople, J. A. *Gaussian 03*, revision C.02; Gaussian, Inc.: Wallingford, CT, 2004.

(28) Bouwstra, J. A.; Schouten, A.; Kroon, J. *Acta Crystallogr., Sect. C* **1983**, *25*, 3561.

(29) Fliegl, H.; Köhn, A.; Hättig, C.; Ahlrichs, R. *J. Am. Chem. Soc.* **2003**, *125*, 9821.

(30) Briquet, A.; Vercauteren, D. P.; André, J.-M.; Perpète, E. A.; Jacquemin, D. *Chem. Phys. Lett.* **2007**, *435*, 257.

(31) Briquet, A.; Vercauteren, D. P.; Perpète, E. A.; Jacquemin, D. *Chem. Phys. Lett.* **2006**, *417*, 190.

(32) Jacquemin, D.; Perpète, A.; Scuseria, G. E.; Ciofini, I.; Adamo, A. *Chem. Phys. Lett.* **2008**, *465*, 226.

(33) Andersson, J.-A.; Petterson, R.; Tegner, L. J. *J. Photochem.* **1982**, *20*, 17.

(34) Dreuw, A.; Head-Gordon, M. *Chem. Rev.* **2005**, *105*, 4009.

(35) Chai, J.-D.; Head-Gordon, M. *J. Chem. Phys.* **2008**, *128*, 084106.

(36) Chai, J.-D.; Head-Gordon, M. *Phys. Chem. Chem. Phys.* **2008**, *10*, 6615.

(37) Yanai, T.; Tew, D.; Handy, H. *Chem. Phys. Lett.* **2004**, *393*, 51.

(38) Peach, M. J. G.; Benfield, P.; Helgaker, T.; Tozer, D. J. *Chem. Phys.* **2008**, *128*, 044118.

(39) Peach, M. J. G.; Ruth Le Sueur, C.; Ruud, K.; Guillaume, M.; Tozer, D. J. *Phys. Chem. Chem. Phys.* **2009**, *11*, 4465.

(40) Jacquemin, D.; Perpète, E. A.; Vydrov, O. A.; Scuseria, G. E.; Adamo, A. J. *Chem. Phys.* **2007**, *127*, 094102.

(41) Kwasniewski, S. P.; François, J. P.; Deleuze, M. S. *Int. J. Quantum Chem.* **2001**, *85*, 557.